# Source parameters of the 7 September 1999 Athens (Greece) earthquake based on teleseismic data

Eleni Louvari and Anastasia Kiratzi

Geophysical Laboratory, Aristotle University of Thessaloniki, 540 06 Thessaloniki, Greece (e-mail: kiratzi@geo.auth.gr)

*Abstract: Far-field body waveform modeling and displacement spectral analysis are used to study the source parameters of the 7 September 1999 Athens earthquake (M $_w$=5.9). The earthquake was caused by the motion of a high-angle normal fault with strike=115°, dip=57°, rake=-80°, auxiliary plane with strike=277° , dip=34°, rake=-105°. The source time function reveals source duration of 4.2 sec, while more than 95% of the energy was abruptly released within the first 2.2 sec. The scalar seismic moment was found equal to 9.22\*10$^{17}$ Ntm. It is worth noting that the fault plane strikes in a WNW-ESE direction, having a small left lateral component of motion. The nearby Atalanti fault, which moved during the 1894 earthquake sequence, and caused severe damage to Athens, has about the same strike orientation. The spectral analysis, assuming a rectangular fault, yielded a fault length L=18 km, fault width w=10 km, stress drop Δσ =9 bars, and average dislocation û=30 cm. These values are in agreement with those expected from the empirical scaling relations applicable to Greece.*

*Key Words: Focal mechanism; Source parameters; Athens earthquake; Greece*

## INTRODUCTION

On 7 September 1999 at 11:56:50 GMT an earthquake of Mw=5.9 struck the capital of Greece, Athens. The epicenter of the event was located at the southwestern flank of Mount Parnitha, around 20 km from the center of the city. Many houses and factories collapsed, the majority of them located within a radius of 12 km from the epicenter, causing the death of 143 people and injuries to more than 2000 (Anastasiadis et al., 1999; Psycharis et al., 1999). This earthquake is of great importance not only because it struck the capital of Greece, with almost 4 million inhabitants, but also because no big earthquake at a distance of less than 30 km has affected so far Athens according to historical records. (Makropoulos et al., 1989; Papazachos and Papazachou, 1997). Figure 1 shows the location of the 7 September 1999 earthquake (Papazachos et al, 1999, personal communication), and all the earthquakes of magnitude M≥6.0 that occurred in the broader region during the time period 1321-1999 (Papazachos and Papazachou, 1997).

The seismic history of Athens spans 25 centuries (Papazachos and Papazachou, 1997; Ambraseys, 1999). Historical records include an account of rather severe earthquake damage to the city of Athens on September 3, 1705. On April 20 and 27, 1894, two large events of magnitude 6.4 and 6.7, respectively, that

occurred at the Atalanti fault, caused minor damage to several buildings and ancient monuments in the city. The 1981 Alkionides (Corinth Gulf) earthquake sequence caused severe damage to 500 buildings and minor damage to the Parthenon. No buildings collapsed and no casualties were reported in Athens. The lack of historical reports of heavy earthquake damage in Athens, and the fact that many ancient monuments in the city are still standing, resulted in the placement of Athens in the zone of low seismicity in the seismic code of 1959. The latest seismic code, adopted in 1995, places Athens in a higher seismic zone (Zone II), where the effective peak ground acceleration is 0.16 g.

The main tectonic structures in the area have an E-W and NW-SE trend. Two neotectonic faults can be identified in the epicentral area: the Aspropyrgos fault, with an azimuth of N120°, and the Fili fault, with an azimuth of N130° (IGME, Geological Map; Tselentis and Zahradnik, 2000). Both faults are associated with an abrupt change in the topographic relief and can be clearly recognized on satellite images. Field work conducted immediately after the mainshock did not identify typical fault traces (Pavlides et al., 1999). Instead, widespread rock falls and gravitational cracks have been observed and mapped especially along the Fili fault and the southwestern Aspropyrgos fault (Pavlides et al., 1999). Furthermore, the aftershock distribution and the vertical cross sections indicate that

most probably the Athens 1999 earthquake was associated with the Fili fault (Tselentis and Zahradnik, 2000) (fig. 1).

The aim of this paper is to study in detail the source parameters of this earthquake, such as its strike, dip, and rake of fault plane, fault length, stress drop and average displacement across the fault, using teleseismic

data from the Global Seismograph Network (GSN). The estimated values of the fault length and stress drop can significantly vary based on the assumed fault geometry. We computed the corresponding values for a circular, rectangular and elliptical fault model, though our results actually indicated that the rectangular model is the most appropriate one.



FIG. 1. A general location map of Athens. Triangles represent the earthquake epicenters of the earthquakes with magnitude M≥6.0 that occurred in the time period 1321-1999 (Papazachos and Papazachou, 1997). The rhombus shows the location of the 7 September1999 Athens earthquake (Papazachos *et al.*, 1999, personal communication). Faults are plotted as solid lines (Jackson *et al.*, 1982; Papanikolaou *et al.*, 1988; Van Andel *et al.*, 1993; Armijo *et al.*, 1996). Contours are every 500 m.

## TELESEISMIC WAVEFORM MODELING

### Method of analysis

The source parameters of the 7 September 1999 Athens earthquake ($M_w$ = 5.9) were calculated using teleseismic body- waveform modeling (McCaffrey *et al.*, 1991). The data used in the inversion consisted of digital P- and SH- waveforms (all having a sampling frequency of 1 Hz), recorded at stations of the Global Seismograph Network (GSN). Following the terminology of FDSN (the Federation of Digital Seismograph Networks) station book proposed by IRIS (the Incorporated Research Institutions of Seismology) we consider these waveforms Long-Period. However, in order to have a better estimate of the source depth and the source time function, we also used P- waveforms

having a sampling frequency of 20 Hz. Following the FDSN station book these waveforms are considered Broad-Band. The waveforms from stations in the epicentral distance range of 30° to 90° were only used in the inversion. P-wave first motion polarities from stations closer than 30° were additionally read to further constrain the nodal planes.

Originally, an FIR (Finite Impulse Response) band pass filter was applied to the data (Oppenheim and Schafer, 1989), in order to remove the high frequency noise. The corner frequencies of the filter were determined by visually comparing the FFT amplitude spectrum of the signal with that of the noise. For most cases the valuable frequency content of the waveforms was lying approximately in the frequency band $f_1 = 0.01$ Hz and $f_2 = 0.2$ Hz for the Long-Period waveforms and $f_1 = 0.1$ Hz and $f_2 = 2$ Hz for the Broad-Band ones.
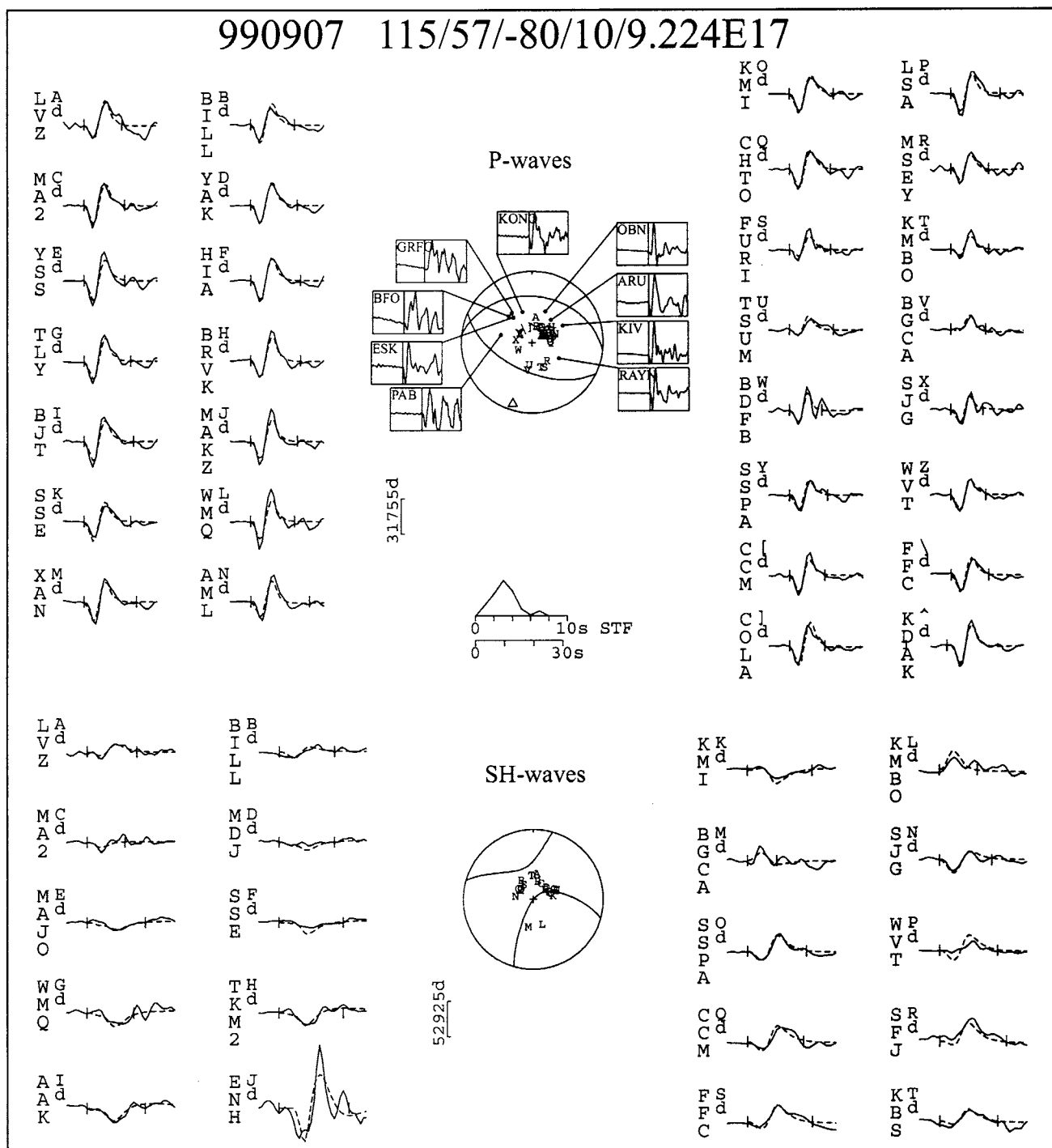
**FIG. 2a.** Comparison between observed (solid line) and synthetic (dashed line) P- and SH Long-Period waveforms (with sampling frequency of 1 Hz). Event header gives strike, dip, rake (in degrees), the depth (in Km) and the seismic moment (in Nm). Lower hemisphere projection is used. P and T axes are marked by solid and open triangles, respectively. Stations are ordered clockwise by azimuth and the station code of each waveform is accompanied by a letter corresponding to its position within the focal sphere. Waveform amplitudes are normalized at a distance of 40° and a gain of 6000. Solid bars at either end of the waveform mark the inversion window. STF is the source time function and the waveform time scale is shown below it. Waveform amplitude scales (in microns) are to the left of the focal sphere. The insets show the first motion polarities at stations with epicentral distances lower than 30°, not included in the inversion but complimentary used to constrain the nodal planes.
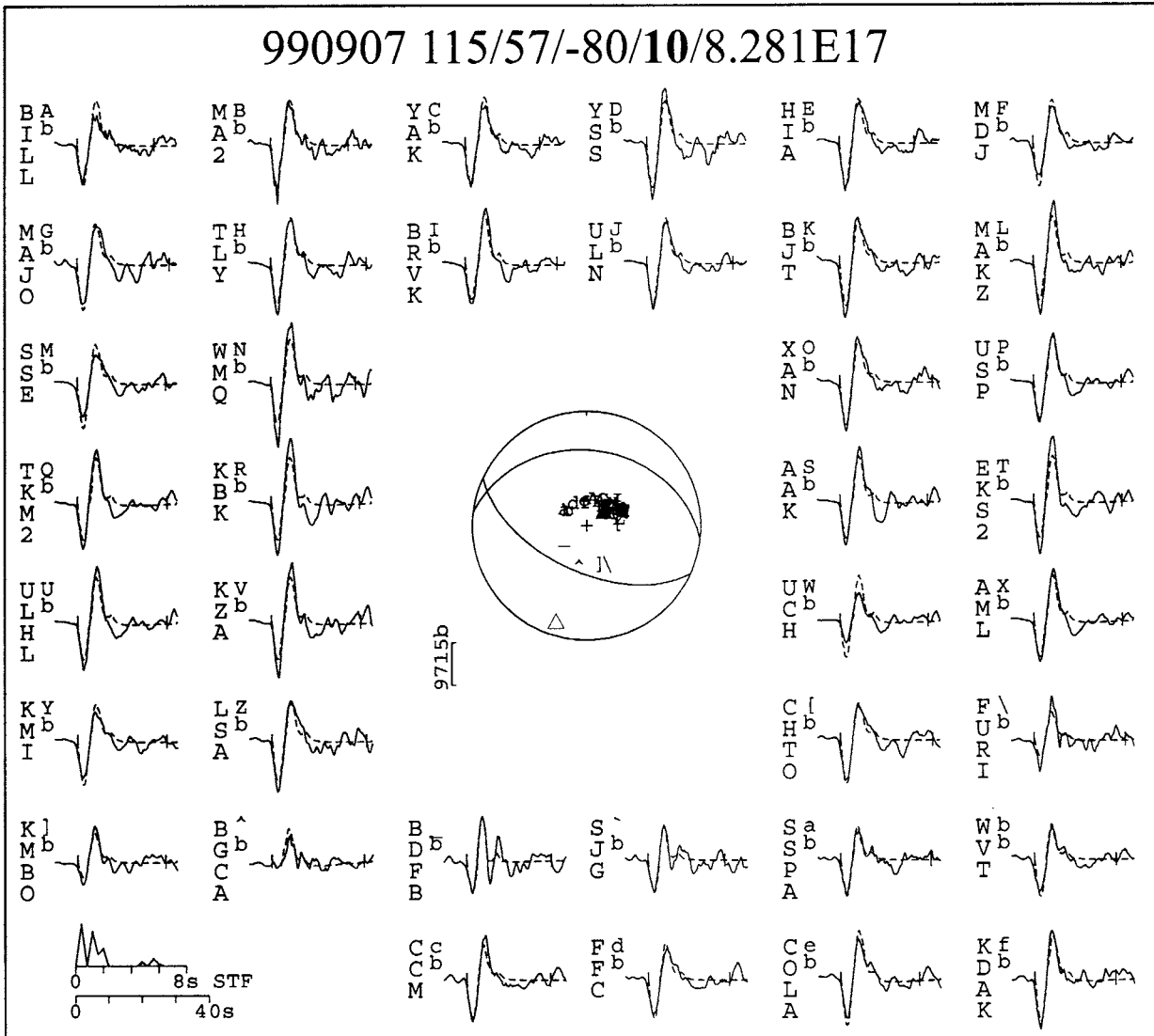
**FIG. 2b.** Comparison between observed (solid line) and synthetic (dashed line) P- Broad-Band waveforms (with sampling frequency of 20 Hz - interpolated at 5 Hz). Notation as in FIG. 2a.

Therefore these frequencies were used as corner frequencies of the filter. All waveforms were converted into displacement records before performing the inversion.

Synthetics were generated for a point source buried in a half space. We used a P-wave velocity of 6.5 km/sec, S-wave velocity of 3.7 km/sec and density 2.8 g/cm³. The receiver structure is assumed to be a homogenous half-space. The instrument response was taken into account by considering the poles and zeros of the system frequency response. The source time function is described by the amplitudes of a series of overlapping symmetrical triangular pulses whose number and duration we selected. The inversion routine yields amplitudes for each triangular shape. Amplitudes were adjusted for geometrical spreading, a simple function of epicentral

distance (Langston and Helmberger 1975), and for attenuation using Futterman's (1962) operator with t* = 1s for P and t* = 4s for SH. The inversion aims to find the "minimum misfit solution" for the strike, dip, rake, depth, and scalar moment between the synthetics and the observed seismograms in a weighted least square's sense. Concerning the error estimates, it has been shown that the covariance matrix associated with this solution usually underestimates the true uncertainties of the determined source parameters (McCaffrey and Nabelĕk, 1987). Thus, in order to find more realistic uncertainties, we follow the procedure of McCaffrey and Nabelĕk, (1987) and Molnar and Lyon-Caen, (1989). In this procedure one simply fixes the source parameters at values close to those obtained from the "minimum misfit solution" allowing all the others to be found by
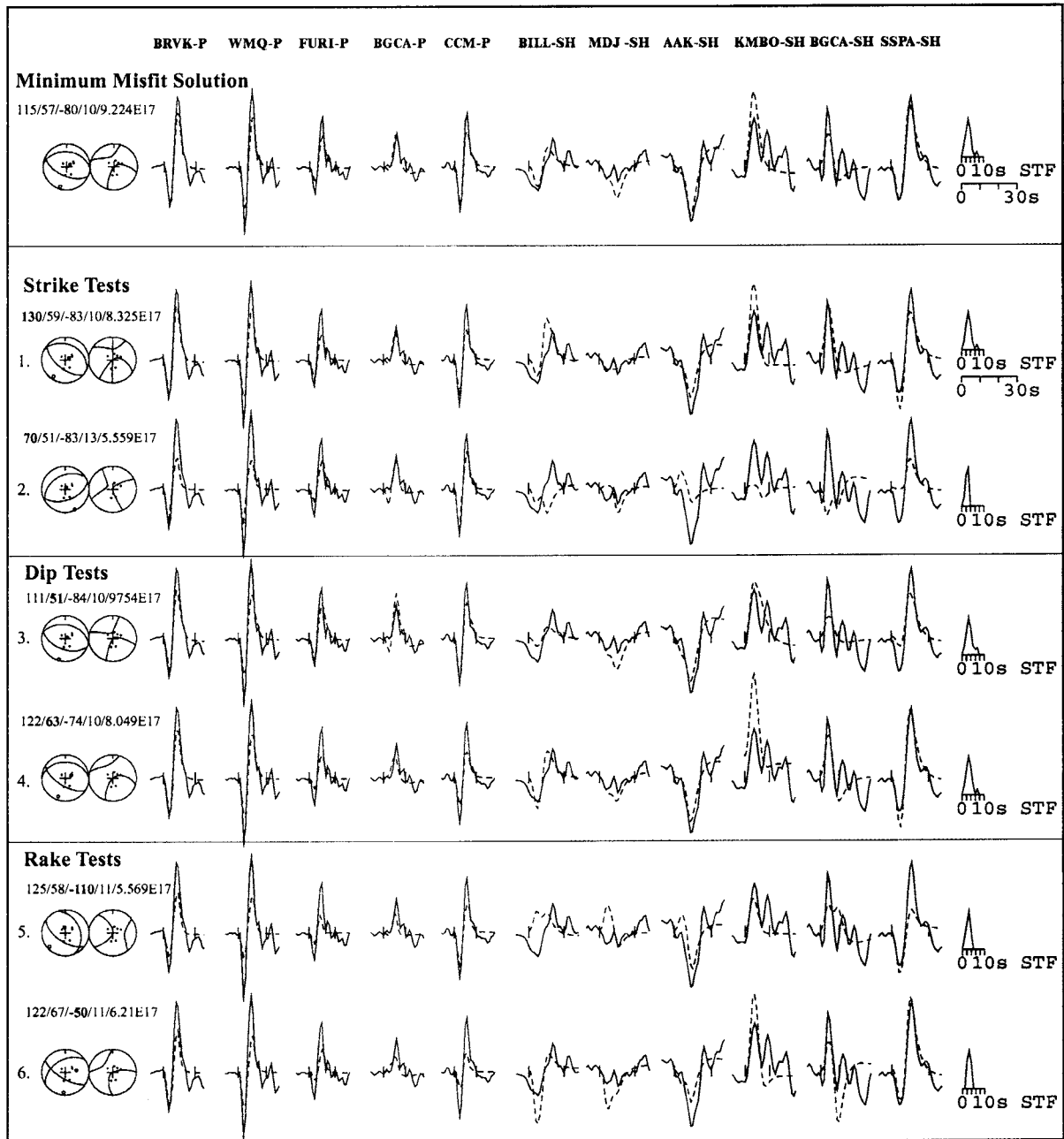
**FIG. 2c.** Various tests to define the uncertainties in the strike, dip and rake (see text for further details).

the inversion routine. Consequently, the errors are found by visual examination where the match of the observed-to-synthetic seismograms significantly deteriorates.

## Inversion Results

30 P- and 20 SH- Long-Period waveforms were used in order to compute the fault plane solution of the 7 September1999 earthquake, which indicates normal faulting along WNW- ESE trending planes (Nodal Plane 1: strike = 115°, dip = 57°, rake = -80°, Nodal Plane 2: strike = 277°, dip = 34°, rake = -105°) (Fig. 2a). First motion polarities from P- waves recorded at 9 stations with epicentral distances Δ<30° are compatible with this solution (inset in fig. 2a). This inversion yielded a source time function with two triangularly shaped pulses. The first one is larger both in amplitude and length (~ 6 sec), while the second one has a length of ~2 sec and an amplitude of just ~10% of the first one. This characteristic shape is observable in all P-waveforms at all azimuths.

**Table 1. Source parameters of the 1999 Athens earthquake derived from body-waveform modeling ξ =azimuth, δ=dip, λ =rake). The numbers in the brackets indicate the lower and the upper bounds of the uncertainties.**

| N | Date (ymd) | Time (h:m) | Lat. (°) | Lon. (°) | $M_w$ | Mox10^17 (Ntm) | Depth (km) | 1st Plane $\xi_1$ (°) | 1st Plane $\delta_1$ (°) | 1st Plane $\lambda_1$ (°) | 2nd Plane $\xi_2$ (°) | 2nd Plane $\delta_2$ (°) | 2nd Plane $\lambda_2$ (°) | P Axis $\xi/\delta$ (°) | T Axis $\xi/\delta$ (°) |
|---|---|---|---|---|---|---|---|---|---|---|---|---|---|---|---|
| 1 | 990907 | 11:56 | 38.06 | 23.54 | 6.0 | 9.224 | 10 (+2/-3) | 115 (+15/-10) | 57 (+5/-2) | -80 (+5/-15) | 277 | 34 | -105 | 54/76 | 198/12 |

As was previously mentioned, the broad-band records are particularly suitable in order to obtain a more refined source depth and source time function. Thus, a better resolve of the source depth and of the source time function was obtained using the broad-band P-waveforms (20 Hz sampling frequency). Due to computer memory limitations, the waveforms were decimated to a sampling frequency of 5 Hz. By fixing the strike, dip and rake of the fault plane at the values previously determined and allowing the depth and the source time function to vary during the inversion, we computed a source depth of 10 km which is in very good agreement with the depth obtained by Tselentis and Zahradnik (2000). The source time function and the fit between the observed and synthetic seismograms of these waveforms are shown in Figure 2b. The focal mechanism parameters of the earthquake modeled as well as the uncertainties are listed in Table 1.

Figure 2c summarizes some of the tests that we have carried out in order to investigate the errors of our minimum misfit solution. Tests 1 and 2 show the comparison between the observed and the synthetic seismograms when the strike was fixed during the inversion at values, each side of value obtained by the minimum misfit solution. Accordingly, in tests 3 and 4 we fixed the dip during the inversion and in tests 5 and 6 we fixed the rake.

## SOURCE PARAMETERS FROM TELESEISMIC BODY WAVE SPECTRA

### Method of analysis

Source parameters, such as seismic moment, fault length, average displacement across the fault and stress drop, were determined using far-field P–wave displacement spectra. The data used consist of Long-Period P-waves (sampling frequency of 1 Hz) recorded at teleseismic distances 30°-90° from the GSN stations. The displacement waveforms were corrected for the instrument response and for attenuation (Futterman, 1962). A time window starting at the P-arrival and ending before the S-arrival was used in order to include amplitudes comparable to the maximum amplitudes of the P-wave train. The radiation pattern was also taken into account and all waveforms were accordingly corrected. The radiation pattern was determined based on the fault plane solution as was previously derived from the body waveform modeling. For those stations with a radiation pattern less than 0.1 seismic moments were not calculated because it would be too large (Hanks and Wyss, 1972).

Almost all far-field displacement spectra were characterized by a constant low-frequency level, $\Omega_o$, and a fall-off above a corner frequency, $f_c$, at a rate proportional to $f^y$. Spectra that did not show such a shape were not analyzed. Determination of the spectral parameters ($\Omega_o$, $f_c$) was performed by eye fitting low- and high-frequency asymptotes to the observed spectra.

The scalar seismic moment was calculated from the relation (Keilis-Borok, 1960):

$$M_o(P) = \frac{\Omega_o(P)}{\Re_{\theta\varphi}(P)} 4\pi\rho Ra^3 \tag{1}$$

where $\Omega_o(P)$ denotes the low-frequency asymptote, $\rho$ the density, $\Re_{\theta\varphi}(P)$ the radiation pattern coefficient for P-waves from a double-couple point source, $R$ the epicentral distance in km and $a$ the P-wave velocity at the source.

Two models were used in order to calculate the source dimensions and the stress drop. At first a circular fault was assumed of radius $r$. Based on Brune (1970, 1971) (as extended by Hanks and Wyss, 1972) the radius of the source is given by relation (2.1), by relation (2.2) following Madariaga (1976) and by relation (2.3) following Sato and Hirasawa (1973):

Brune model $\qquad r(P) = \dfrac{0.37a}{f_{c_p}} \qquad (2.1)$

Madariaga model $\qquad r(P) = \dfrac{0.32\beta}{f_{c_p}} \qquad (2.2)$

Sato and Hirasawa model $\qquad r(P) = \dfrac{0.24a}{f_{c_p}} \qquad (2.3)$

where $f_{cp}$ is the corner frequency of P-wave spectra and $\beta$ is the velocity of the S-waves. We have assumed that the diameter of a circular fault area should be equal to the observed fault length (Hanks and Wyss, 1972). Stress drop, $\Delta\sigma$, was calculated from the relation (Kelis-Borok, 1959; Brune, 1970, 1971):
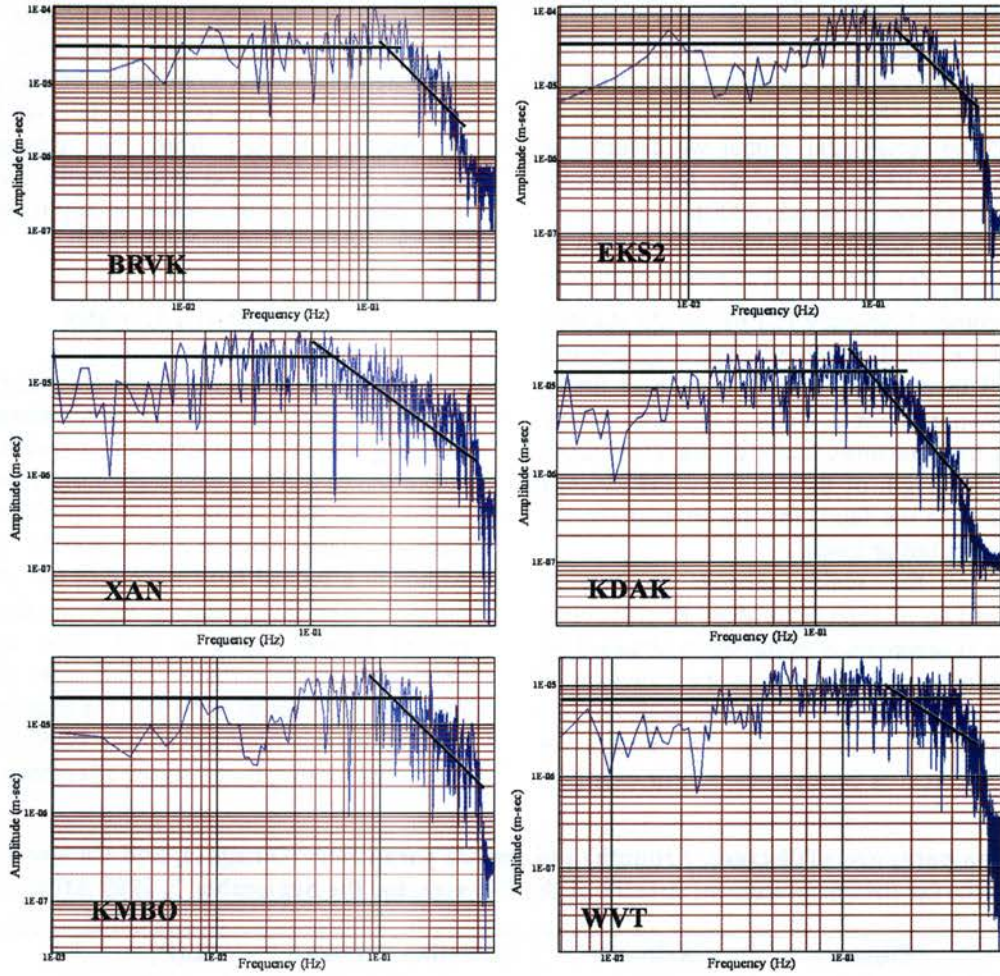
**FIG. 3.** Far-field displacement amplitude spectra for the 7 September1999 Athens earthquake. Displacement waveforms have been corrected for instrument response, attenuation, and the radiation pattern. The low and high frequency asymptotes (straight lines) were fitted by eye.

$$\Delta\sigma = \frac{7}{16}\frac{M_0}{r^3} \qquad (3)$$

Based on the second model, a bilateral rupture over a rectangular area of fault width, W, and fault length, L, was considered (Savage, 1972, 1974). Assuming a constant value of width (W), the calculation of the fault length (L) is based on the relation (4) which holds for P- waves (Aki and Richards, 1980).

For this model and for a dip slip fault the stress drop, $\Delta\sigma$, is (Aki, 1966):

$$\Delta\sigma = \frac{8Mo}{3\pi LW^2} \qquad (4)$$

The average displacement, $\bar{u}$, across the fault was calculated from the relation (Aki, 1966):

$$M_0 = \mu A\bar{u} \qquad (5)$$

where $\mu$ is the shear modulus and $A$ is the fault surface.

Average values $\langle x \rangle$ were computed for each parameter (stress drop, fault length, average displacement) following Archuleta *et al.* (1982):

$$\langle x \rangle = \text{antilog}\left(\frac{1}{N}\sum_{i=1}^{N}\log x_i\right) \qquad (6)$$

where $N$ is the number of stations used. The basic reason is that in the case of simple arithmetic average the mean values would be biased towards the larger values. The corresponding standard deviation of the logarithm $SD(\log\langle x \rangle)$ and the multiplicative error factor, Ex, were calculated from the relations (Garcia-Garcia *et al.*, 1996):

$$SD(\log\langle x \rangle) = \left[\frac{1}{N-1}\sum_{i=1}^{N}(\log x_i - \log\langle x \rangle)^2\right]^{1/2} \qquad (7.1)$$

$$Ex = \text{antilog}(SD(\log\langle x \rangle)) \qquad (7.2)$$

## Source parameters from the spectral analysis

For all the calculations we used a value of 6.5 km/sec for the velocity of the P-waves, a density of 2.6 g/cm$^3$ and a value 3.3 Nt/m$^2$ for the shear modulus, $\mu$. In the case of the rectangular model we assumed a fault width (W) of 10 km, based on the aftershock distribution (Tselentis and Zahradnik, 2000).

The distance, the azimuth, the radiation pattern of the P-waves ($\Re_{\theta\varphi}(P)$), the low frequency asymptote ($\Omega_o$) and the corner frequency (f$_c$) of the 25 stations that were used are listed in Table 2. The displacement spectra of 6 of them, together with their best fitting results, are shown in figure 3. Table 3 lists the average values and the multiplicative factor of the stress drop, the radius or the length of the fault and the average displacement across the fault, for the circular model, as well as the rectangular model.

The value of the scalar seismic moment is determined based on relation (1) is Mo=1.82×1018 Ntm, which is larger in comparison to the value obtained by the body waveform modeling due to the inclusion of the whole spectrum of the P-waves in the analysis.

By comparing the results of the two models we observe large differences between them. For example,

the Brune circular model results in a fault length of 36 km (2*radius), considerably overestimated as compared to the other models. At any rate, even though we calculated the source parameters for the 1999 Athens mainshock using a variety of models, we finally adopt the results obtained from the rectangular model because they are in agreement with those expected from empirical scaling relations applicable to Greece (Papazachos and Papazachou, 1997).

## CONCLUSIONS

Source parameters for the 7 September1999 Athens earthquake were determined using teleseismic waveform modeling and far-field displacement spectra. The earthquake was caused by a high angle normal fault with parameters: Fault plane: strike = 115o, dip = 57o, rake = -80°, auxiliary plane: strike = 277°, dip = 34°, rake = -105°. Although a typical fault trace was not observed after the earthquake, fault mapping, intensity distribution and ground failures (such as rock falls, separations in preexisting faults surfaces, small scale landslides and local ground fissures) imply that the most probable fault is the Fili fault (Pavlides *et al.*, 1999). Tselentis and Zahradnik (2000), based on the aftershock distribution,

**Table 2. Station parameters (Distance, Azimuth) and spectra parameters (Omega-$\Omega_o$ and Corner Frequency-$f_c$) obtained from the far field displacement spectra of the P-waves, for the September 7, 1999 Athens earthquake.**

| Station (code) | Distance (km) | Azimuth (o) | Radiation Pattern $\Re_{\theta\varphi}(P)$ | $\Omega_o(P)$ (m-sec) | $f_c$ (Hz) |
|---|---|---|---|---|---|
| BILL | 4702 | 14 | 0.411 | 1.43E-05 | 0.122 |
| MA2 | 5361 | 25 | 0.432 | 1.99E-05 | 0.118 |
| YAK | 4559 | 30 | 0.356 | 2.00E-05 | 0.139 |
| HIA | 5277 | 46 | 0.411 | 1.95E-05 | 0.116 |
| TLY | 4363 | 48 | 0.330 | 2.05E-05 | 0.109 |
| BRVK | 2735 | 50 | 0.182 | 2.97E-05 | 0.125 |
| BJT | 5876 | 56 | 0.474 | 1.98E-05 | 0.107 |
| MAKZ | 3516 | 59 | 0.290 | 3.02E-05 | 0.138 |
| XAN | 5940 | 64 | 0.508 | 1.90E-05 | 0.122 |
| TKM2 | 3304 | 66 | 0.327 | 3.44E-05 | 0.112 |
| KBK | 3274 | 67 | 0.328 | 4.06E-05 | 0.115 |
| AAK | 3248 | 67 | 0.329 | 3.40E-05 | 0.107 |
| EKS2 | 3203 | 67 | 0.327 | 3.91E-05 | 0.157 |
| ULHL | 3370 | 67 | 0.339 | 2.99E-05 | 0.115 |
| KZA | 3316 | 67 | 0.338 | 3.02E-05 | 0.126 |
| ENH | 6287 | 68 | 0.545 | 2.50E-05 | 0.110 |
| KMI | 6243 | 76 | 0.580 | 1.65E-05 | 0.131 |
| CHTO | 6481 | 83 | 0.637 | 1.71E-05 | 0.132 |
| KMBO | 4225 | 159 | 0.917 | 2.01E-05 | 0.119 |
| BGCA | 3352 | 190 | 0.831 | 1.48E-05 | 0.146 |
| SSPA | 6308 | 309 | 0.676 | 8.06E-06 | 0.167 |
| WVT | 7277 | 311 | 0.704 | 7.15E-06 | 0.152 |
| FFC | 5851 | 331 | 0.590 | 9.05E-06 | 0.176 |
| COLA | 5335 | 356 | 0.501 | 1.01E-05 | 0.181 |
| KDAK | 6280 | 358 | 0.544 | 1.53E-05 | 0.157 |

**Table 3. Mean values of the stress drop, radius or length of the fault and the average displacement across the fault for the models examined $E_{\Delta\sigma}$ = multiplicative factor for the stress drop, $E_L$= multiplicative factor for the fault length, $E_u$ = multiplicative factor for the average displacement across the fault.**

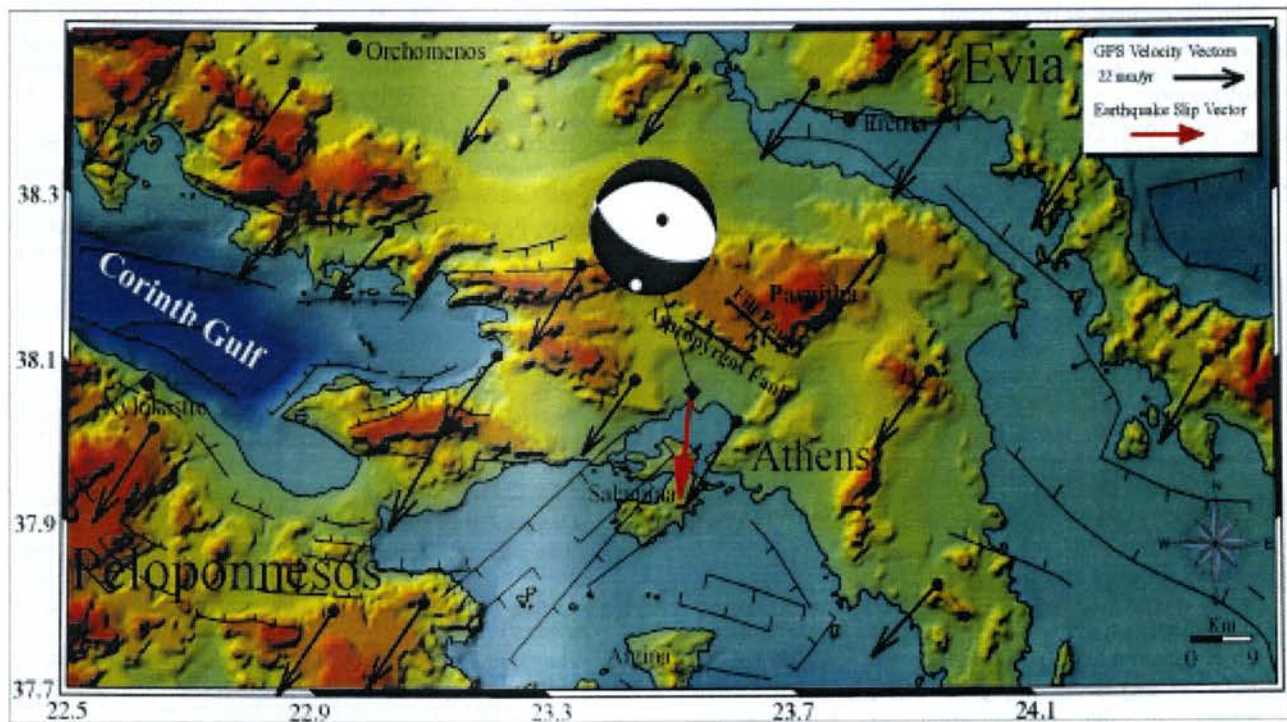| | Stress Drop (bar) | $E_{\Delta\sigma}$ | Fault Length (km) | $E_L$ | Displacement (cm) | $E_u$ |
|---|---|---|---|---|---|---|
| Circular Model (Brune) | 1.24 | 1.64 | 37 | 1.17 | 5 | 1.61 |
| Circular Model (Madariaga) | 11.52 | 1.64 | 18 | 1.17 | 22 | 1.61 |
| Circular Model (Sato & Hirosawa) | 4.44 | 1.64 | 24 | 1.17 | 12 | 1.61 |
| Rectangular Model | 8.45 | 1.37 | 18 | 1.37 | 30 | 1.61 |



**FIG. 4**. Fault plane solution of the 7 September1999 Athens earthquake (lower hemisphere projection) plotted on the Digital Elevation Model (DEM) of the area. Vectors represent the GPS horizontal velocities with respect to stable Eurasia (Davies *et al.*, 1997; Clarke *et al.*, 1998; McClusky *et al.*, 2000).

proposed that the fault plane has an azimuth of 117° and a dip of 52°, which is in very good agreement with our results. According to the same authors the continuation of this fault plane upwards intersects the earth surface along the Fili fault.

Far-field displacement spectra were used to calculate source parameters. Circular and rectangular fault models were tested and the results finally adopted for a rectangular fault give a fault length 18 km, a width of 10 km, average displacement across the fault of 30 cm, and stress drop of 9 bars. Figure 4 shows the fault plane solution of the 7 September 1999 earthquake and the slip vector of the SW dipping plane, which is in a rather good agreement with the GPS horizontal velocities referenced to stable Eurasia.

**ACKNOWLEDGEMENTS**

**REFERENCES**

Aki, K., 1966. Generation and propagation of G-waves from the Niigata earthquake of June 16, 1964. Part 2. Estimation of earthquake moment, released energy, and stress-strain drop from the G-waves spectrum: Bull Earthquake Res. Inst., Tokyo Univ., **44**, 73-88.

Aki, K. and Richards, P., 1980. Quantitative Seismology: Theory and methods. Freeman, San Francisco, Calif., 557 p.

Ambraseys, N., 1999. Material for the investigation of the seismicity of central Greece. (http://emidius.irrs.mi.cnr.it/RHISE/ii_lamb//ii_lamb.html).

Archuleta, R. J., Cranswick, E., Mueller, Ch and Spudich, P., 1982. Source parameters of the 1980 Mammoth lakes, California, earthquakes sequence: J. Geophys. Res., **87**, 4595-4607.

Armijio, R., Meyer, B., King, G. C. P., Rigo, A. and Papanastasiou, D., 1996. Quaternary evolution of the Corinth Rift and its implications for the Late Cenozoic evolution of the Aegean: Geophys. J. Int., **126** , 11-53.

Anastasiadis, An., Demosthenous, M., Karakostas, Ch., Klimis, N., Lekidis, B., Margaris, B., Papaioannou, Ch., Papazachos, C. and Theodoulidis, N., 1999. The Athens (Greece) earthquake of Septhember 7, 1999: Preliminary report on strong motion data and structural response. (http://www/itsak.gr/report.html).

Brune, J. N., 1970. Tectonic stress and the spectra of seismic shear waves from earthquakes: J. Geophys. Res., **75**, 4997-5009.

Brune, J. N., 1971. Correction (to Brune (1970): J. Geophys. Res., **76**, 5002.

Clarke, P. J., Davies, R. R., England, P. C., Parsons, B., Billiris, H., Paradissis, D., Veis, G., Cross, P. A., Denys, P. H., Ashkenazi, V., Bingley, R., Kahle, H.-G., Muller, M.-V. and Briole, P., 1998. Crustal strain in central Greece from repeated GPS measurements in the interval 1989-1997: Geophys. J. Int., **135**, 195-214.

Davies, R., England P., Parsons, B., Billiris, H., Paradissis, D. and Veiss, G., 1997. Geodetic strain of Greece in the interval 1892-1992: J. Geophys. Res., **102**, 24571-24588.

FDSN, Station Book produced by Incorporated Research Institutions for Seismology. (http:// www.iris.washington.edu/GSN).

Futterman, W. I., 1962. Dispersive body waves: J. Geophys. Res., **67**, 5279-5291.

Garcia-Garcia, J. M., Vidal, F., Romacho, M. D., Martin-Marfil. J. M., Posadas, A. and Luzon, F., 1996. Seismic source parameters for microearthquakes of the Granada basin (southern Spain): Tectonophysics, **261** , 51-66.

Hanks, T. C. and Wyss, M., 1972. The use of body-wave spectra in the determination of seismic-source parameters: Bull. Seism. Soc. Am., **62**, 561-589.

IGME – Institute of Geological and Mineralogical Research. Geological Map, 1:500 000 scale.

Jackson, J., Gagnepain, J., Houseman, G., King, G. C. P., Papadimitriou, P., Soufleris, C. and Virieux, J., 1982. Seismicity, normal faulting and the geomorphological development of the Gulf of Corinth (Greece): The Corinth earthquakes of February and March 1981: Earth Planet. Sci. Lett., **57**, 377-397.

Keilis-Borok, V. I., 1959. An estimation of the displacement in an earthquake source and of source dimensions: Ann. Geofis., **12**, 205-214.

Keilis-Borok, V. I., 1960. Investigation of the mechanism of earthquakes: Sov. Res. Geophys., **4**, 29.

Langston, C. and Helmberger, D. V., 1975. A procedure for modeling shallow dislocation sources: Geophys. J. Roy. Astr. Soc., **42**, 117-130.

Macropoulos, K., Drakopoulos, J. and Latousakis, J., 1989. A revised and extended earthquake catalog for Greece since 1900: Geophys. J. Int., **98**, 391-394.

Madariaga, R., 1976. Dynamics of the expanding circular fault: Bull. Seism. Soc. Am., **66**, 639-666.

McCaffrey, R. and Nabel ĕk, J., 1987. Earthquakes, gravity, and the origin of the Bali Basin: an example of nascent continental fold-and-thrust belt: J. Geophys. Res., **92**, 441-460.

McCaffrey, R., Abers, G. and Zwick, P., 1991. Inversion of Teleseismic Body Waves: International Association of Seismology and Physics of the Earth's Interior, p. 166.

McClusky, S., Balassanian, S., Barka, A., Demir, C., Georgiev, I., Hamburg, M., Hurst, K., Kahle, H., Kastens, K., Kekelidze, G., King, R., Kotzev, V., Lenk, O., Mahmoud, S., Mishin, A., Nadariya, M., Ouzounis, A., Paradissis, D., Peter, Y., Prilepin, M., Reilinger, R., Sanli, I., Seeger, H., Tealeb, A., Toksoz, M.N. and Veis, G., 2000. Global Positioning System constraints on plate kinematics and dynamics in the eastern Mediterranean and Caucasus: J. Geophys. Res ., **105**, 5695-5720.

Molnar, P. and Lyon-Caen, H., 1989. Fault plane solutions of earthquakes and active tectonics of the Tibetan Plateau and its margins: Geophys. J. Int., **99**, 123-153.

Oppenheim, A. V. and Schafer, R. W., 1989. Discrete-Time Signal Processing: Prentice Hall, USA, 879 p.

Papanikolaou, D. J., Lykousis, V., Chronis, G. and Pavlakis, P., 1988. A comparative study of Neotectonic basins across the Hellenic arc: the Messiniakos, Argolikos, Saronikos and Southern Evoikos Gulfs: Basin Research, **1**, 167-176.

Papazachos, B. C. and Pap azachou, C., 1997. The earthquakes of Greece: Ziti Publications, Thessaloniki, Greece, 304 p.

Pavlides, S., Papadopoulos, G. A. and Ganas, A., 1999. Field Report: The strong earthquake of 7 September, 1999 in Athens. (http://www.earth.ox.ac.uk/~timw/athens/).

Psycharis, I., Papastamatiou, D., Taflambas, I. and Carydis, P., 1999. The Athens, Greece Earthquake of 7 September 1999. EERI Special Earthquake Report, November 1999. (http://www.eeri.org/Reconn/Gr eece 1099).

Sato, T. and Hirasawa, T., 1973. Body wave spectra from propagating shear cracks: J. Physics of the Earth, **21**, 415-431.

Savage, J. C., 1972. Relation of corner frequency to fault dimensions: J. Geophys. Res., **77** , 3788-3795.

Savage, J. C., 1974. Relation between P and S corner frequencies in the seismic spectrum: Bull. Seism. Soc. Am., **64**, 1621-1267.

Tselentis, G.A. and Zahradnik, J., 2000. The Athens earthquake of September 7 1999: Bul. Seism. Soc. Am., **90**, 1143-1160.

Van Andel, T. H., Perissoratis, C. and Rondoyanni, T., 1993. Quaternary tectonics of the Argolikos Gulf and adjacent basins, Greece: J. Geol. Soc. Lon., **150** , 52-59.